

Experimental Study of Current Forces and Deformations on a Half Ellipsoidal Closed Flexible Fish Cage

I.M Strand^{a,*}, A.J Sørensen^a, Z.Volent^b, P.Lader^b

^a*Centre for Autonomous Marine Operations and Systems, Department of Marine Technology,
Norwegian University of Science and Technology, Trondheim, Norway*

^b*SINTEF Fisheries and Aquaculture, Trondheim, Norway*

Abstract

Closed Flexible Fish Cages are proposed as a new concept in marine aquaculture, replacing the conventional net cages in order to meet ecological challenges related to fish lice and escapes. It is important to understand the response of the cage exposed to current loads. Then more knowledge about forces and deformations on the Closed Flexible Fish Cage for different filling levels is needed. A scaled model of a Closed Flexible Fish Cage shaped like a half ellipsoid was tested in a towing-tank. Global drag forces and bag deformations were measured for four different filling levels between 70-100 %, and steady current velocities between 0.04 m/s and 0.22 m/s in model scale, corresponding to Reynolds numbers in the range $Re = 3 - 17 \cdot 10^4$. Findings from the experiments showed that the drag force increased for decreasing filling levels. This increase was caused by a large deformation of the front of the bag affecting the drag coefficient.

Keywords: Aquaculture, hydroelastic, drag, flexible, large deformations

1. Introduction

Norway has become the worlds largest producer of Atlantic salmon through use of open net structures in the sea. The aquaculture facilities have grown both in size and number. Currently, the industry faces increased attention on environmental challenges related to fish escapes, sea-lice, diseases and pollution. This is despite improvements in technology and operational procedures. The aquaculture industry is under a considerable pressure to introduce technologies and practices that reduce the influence from the aquaculture on the environment (Michael et al., 2010). A possible contribution to the solution, is to develop a Closed Flexible Fish Cage (CFFC). The main objective of the CFFC is to better restrict and control the interaction between the fish farm and the surrounding environment.

The CFFC is a membrane structure, replacing the net structure. Remaining parts of the fish farm installation such as the floater and mooring system may be used as before. By reusing available components, the CFFC may be easier to put directly into operation at existing sites. By exchanging the net with a tight bag we get a closed compliant submerged structure with a free surface. Few ocean structures exist with large, compliant submerged components. It is therefore presently limited existing knowledge about how CFFCs will respond to external sea loads (Rosten et al., 2013). It is crucial to secure the cage against structural collapse. Therefore, knowledge of the behaviour of the bag when subjected to current and wave loads is vital. The modelling and investigations of sea loads on CFFCs will start with locations in less exposed waters. We will therefore in the work of this paper only consider current loads.

*Corresponding author at tel.: +47 93 69 44 67.

Email address: `ida.strand@ntnu.no` (I.M Strand)

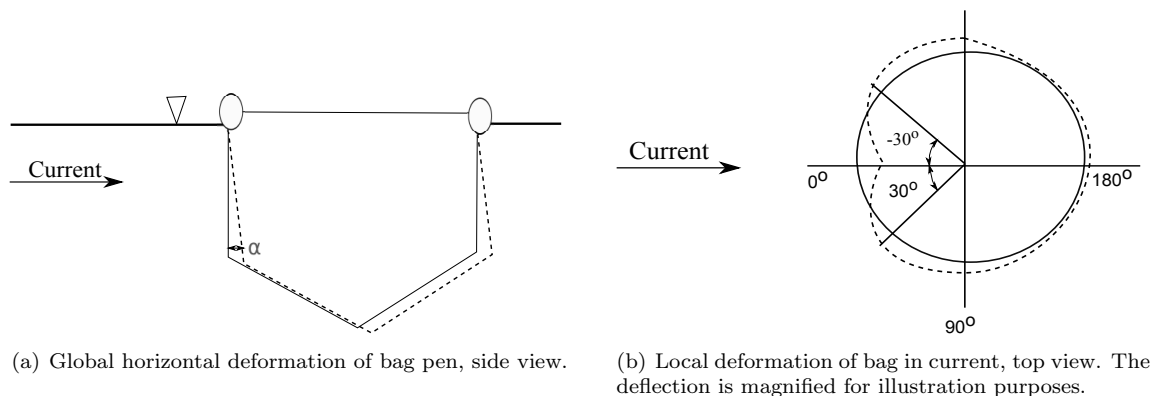


Figure 1: Deformations of a bag pen in current, adapted from Rudi and Solaas (1993).

The bag is flexible and behaves hydro-elastically, meaning that the deformation of, and hydrodynamic forces on the bag are closely coupled. Rudi and Solaas (1993) modelled the effect of current forces and deformation, on a full bag pen, which is an early version of the CFFC. They found both global and local deformation patterns. The global deformation of the bag pen was approximated based on moment equilibrium. A symmetric deformation of both the front and the back wall of the bag were found, comparable to deformations of a rigid beam under pressure, see figure 1(a). Local deformations of the bag wall was approximated based on the varying pressure distribution around a rigid circular cylinder in steady flow. Due to these pressure variations, the front of the bag was pressed inwards in an area of ± 30 deg upstream of the bag, see figure 1(b).

The elasticity of the material and the tension in the fabric govern the shape and flexibility of a fabric structure (Løland and Aarsnes, 1994). Flexible containment bags used for transportation of fresh water or oil in the sea, are the structures that most resembles the CFFC. For the flexible containment bags, it have been found that the shape and tension are strongly dependent on the filling level, as presented in Hawthorne (1961) and Zhao (1995).

The filling level of the bag is defined according to the theoretical full volume of the bag. The main operational condition of the CFFC will be full, or overfilled/inflated. However, there might arise situations where the bag is in a condition where it is less than full. Strand et al. (2013) and Lader et al. (2015) studied experimentally the effect on filling level on the drag force for different geometries. The experiments were conducted in the small towing tank at the US Naval Academy in August 2012. Strand et al. (2013) analysed the results for a cylindrical bag, and Lader et al. (2015) compared four different geometries : a cylindrical bag with a cone at the bottom, a cubical bag with a pyramid at the bottom, a conical bag and a pyramidal bag. Velocities in the range 0.021-0.127 m/s were studied, giving Reynolds numbers on the range $Re = 1 - 8 \cdot 10^4$. The Reynolds number is based on the diameter, and given as $Re = UD/\nu$. The Reynolds number is a non-dimensional measure of the characteristics of the flow regime, D is the diameter, U is the velocity and ν is the kinematic viscosity of the fluid, here fresh water. They found that the drag forces on all the different geometries increased with decreasing filling levels. However, for the cylindrical and cubical bags the drag forces had a larger increase than for the conical and pyramidal bags. This increase in drag was found to be due to a local deformation in the front, apparent for filling levels less than 100%, affecting the drag coefficient unfavourably. This deformation were most pronounced for the cylindrical and cubical structures. The deformation resembled the local deformation pattern given by Rudi and Solaas (1993), only in a larger scale. For Reynolds numbers ($Re > 4 \cdot 10^4$) at filling levels below 90 % the local deformations in the front described by Strand et al. (2013), Lader et al. (2015) and Rudi and Solaas (1993) could resemble the shape of a regular parachute. Even though the parachute is an open volume, and the CFFC is a closed volume and thereby also dependent on the internal flows and motions of the bag, parallels can be drawn. The drag coefficients found for the cylindrical and cubical bag in Strand et al. (2013) and

Lader et al. (2015) were close to the drag coefficient range found for parachutes and hemispherical cups (Hoerner, 1958).

For Reynolds numbers below $Re \leq 4 \cdot 10^4$ (low velocities), the bag did not appear to deform, but remained the shape as it appeared for only static pressure (Strand et al., 2013). The shape of the bag in still water for pure static pressure were found to be dependent on the load history of the bag (Strand et al., 2014). This indicates that the initial shape of the bag can effect the experimental results.

In this paper experimental work considering a half ellipsoidal CFFC with a diameter of 0.75 m, for four filling levels between 70 and 100% and for towing velocities in the range $U = 0.04 - 0.22$ m/s are presented and discussed. The model test data and observations are used to formulate mathematical models of the CFFC in current, in particular drag coefficients are found. This work is a continuation of the work presented in Strand et al. (2013), Strand et al. (2014), and Lader et al. (2015), but considering a different geometry, a larger range of Reynolds numbers, and running longer experimental runs in the towing tank, that is longer travelled distance.

The paper is organized as follows. In chapter 2 the experimental set-up and instrumentation are presented. The experimental results are analysed in section 3. Discussion is given in section 4. Finally, conclusions are given in section 5.

Nomenclature

| | | | |
|----------------------|--|-----------|------------------------------------|
| A | Projected frontal area | L/r | non-dimensional travelled distance |
| C_D | Dimensionless drag coefficient | λ | Filling level |
| $\bar{C}_D(\lambda)$ | Mean drag coefficient for each filling level | ν | Kinematic viscosity of the fluid |
| D | Diameter of the bag | ρ | Fluid density |
| E | Young's Modulus | τ | Froude scale |
| F_D | Drag force | t_F | Thickness of fabric in full scale |
| F_x | Force measurements in x direction | t_M | Thickness of fabric in model scale |
| h | Max draft of the bag | U | Towing velocity |
| h_d | Deformed draft of the bag | V_0 | Full volume of the bag |

2. Experimental set-up and instrumentation

To study the effect of current loads on an half ellipsoidal CFFC, a number of experimental runs of a model scale bag at different filling levels and current velocities were done in the Marine Cybernetics Laboratory (MC-Lab) at NTNU in Trondheim, Norway. All the experiments turned out to be of great importance in the understanding of important physics and in future development and verification of the mathematical models of the CFFC in current.

The MC-Lab is a small towing tank, 40 m long, 6.45 m wide and with a depth varying from 1.4 m to 1.5 m. Experiments were run in March and May 2013. In March, the 70 % and 100 % filling levels were tested. In May, the aim were to repeat the experiments from March and in addition run tests at 80 and 90 % filling levels. In the following the different experimental runs will be designated as March 2013 and May 2013. See figure 2 for model and measurement set-up for the experiment, and table 1 for the test matrix describing the various test runs.

The CFFC consists of three parts: The bag itself, the bag content, and an attachment system. The bag was tailored in a half ellipsoidal shape of ripstop nylon, of thickness 0.05 mm and weight 40 g/m², see table 1 for dimensions. Cotton tread were used in the sewing to reduce the permeability at the seams. A floater placed inside the fabric at the water surface was used as attachment system, inspired by Kristiansen and Faltinsen (2015). The floater was made by a corrugated plastic tube in PVC with diameter 25 mm, a mass of 0.104 kg/m, and stiffened by ropes in the horizontal water plane to avoid ovalization. The floater was connected by four nearly horizontal mooring lines to the carriage in the center line of the tank. The mooring lines were made of 2 mm nylon halyard.

A flow meter with an accuracy of 3 % was used to measure the amount of water in the bag. The Nylon fabric used for the bag model is to some extent permeable giving a net flow through the fabric,

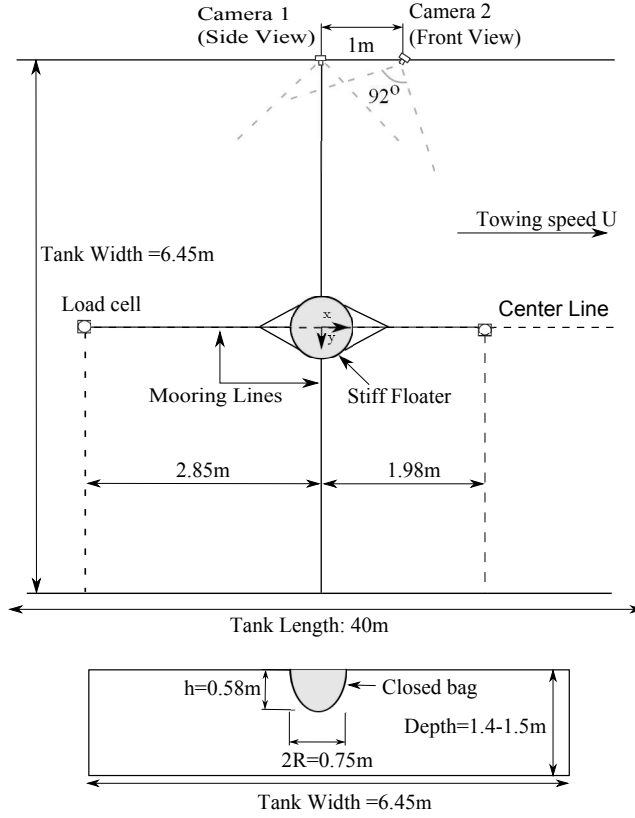


Figure 2: Experimental set-up. Upper: Top view. Lower: Front view. Tank dimensions of the MC-Lab are 40 m \times 6.45 m \times 1.5 m. The Cartesian coordinate system is located at the center of the floater in the free surface. The floater is stiffened in the free surface to avoid ovalisation and is moored by four moorings; front, aft and two side moorings.

when subjected to pressure differences. The intention in the present experiments were that the volume inside the bag should remain constant during the experiments. The amount of water in the bag was measured after each filling level experiment. The leakage out of the bag during the different run series for each filling level was found to be within 3-4 % of the intended filling level.

Current was simulated by towing the model under the carriage, with towing velocities U in the range $U = 0.04 - 0.22$ m/s. The towing carriage were experienced to be steady and accurate for the given velocity range. Kristiansen and Faltinsen (2015) have tested the accuracy of MC-Lab carriage velocity, and found it to be highly steady, and within 0.2% of the desired value, reducing the possibility that an experimental bias introduced by the carriage.

Drag forces were measured in the towing direction by load cells in the front and aft mooring line. The load cells were sampled at 200 Hz. The uncertainty of the load cell was found to be 0.05 N, which is ≥ 10 % of the mean drag force for the two lowest velocities, and ≤ 6 % and decreasing for the higher velocities. Mean drag forces were found by taking the average over 40 seconds of the measurement time interval with the smallest standard deviation, after the initial startup, for each run. This time interval will be referred to as the middling time interval. Each time series were between 90-120 seconds long.

Two underwater cameras of the type Go Pro 3 were used to measure/observe the deformations of the bag. The cameras had a fixed 92 degree wide angle lens (figure 2). One capturing the side of the bag, and the other capturing the front/side. The cameras followed the model during the test attached to the towing carriage. Both cameras were placed to avoid disturbing the incoming current.

Quantitative measures of the geometry of the bag were obtained from the image material. Deformed

Table 1: Test matrix showing dimensions, filling levels, and towing velocities.

D is the diameter of the bag, h is the max draft, V_0 is the full filling level, λ is the filling level of the bag, and U the towing velocity

| | D (m) | h (m) | V_0 (l) | λ (%) | U (m/s) |
|------------|---------|---------|-----------|---------------|--|
| March 2013 | 0.75 | 0.58 | 180 | 70,100 | 0.04, 0.05, 0.07, 0.10, 0.12, 0.15, 0.17, 0.19, 0.22 |
| May 2013 | | | | 70-100 | |

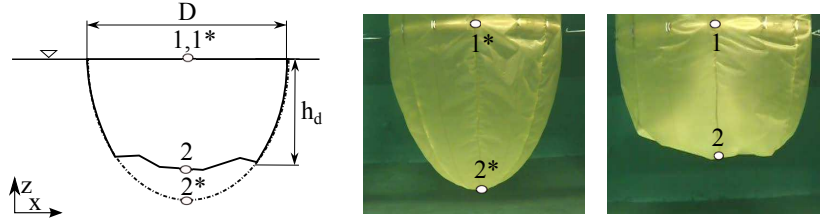


Figure 3: Illustration of marker placement under estimation of deformed draft from images. Left: Sketch of marker placement for the deformed draft (1,2) and reference used for calibration in 100% full images (1*,2*). Middle: Image of 100% full bag used to calculate reference draft (1*,2*), taken by camera 1. Right: Example of marker placement on deformed bag, 70% full bag (1,2).

drafts were calculated for all the current experiments conducted in the MC-Lab. Coordinates of the images from camera 1 (see figure 2), were translated to real world coordinates by an image analysis. In the image analysis coordinates of the waterline and the bottom of the bag were used to estimating a deformed draft of the bag. The 100% filling level images together with the known full draft were used to define a calibration coefficient, to transform the pixel information into length measures. The deformed draft h_d was found according to:

$$h_d = \frac{h}{z_{2^*} - z_{1^*}}(z_2 - z_1), \quad (1)$$

where z_{2^*}, z_{1^*} are the z-coordinates of the reference picture, and z_2, z_1 are the z-coordinates of the deformed draft picture. The points were placed as illustrated in figure 3. The estimated error of the placement of the coordinates are in the order of ± 0.5 cm (± 1 %). This estimated error was found based on the variance of the draft of the 100 % filling level in stationary condition, which is known.

3. Results

The results of the experiments will be analysed in the following subsections. The drag force is known to be dependent on the shape of the structure, and the projected area. The drag force on a structure in uniform flow is given by the drag equation:

$$F_D = \frac{1}{2}\rho AC_D U^2, \quad (2)$$

where ρ is the fluid density, which is equal to 1000 kg/m^3 for fresh water, and A is the projected frontal area. The drag coefficient C_D is dependent of the shape of the body, the flow regime around the body and the Reynolds number.

3.1. Force measurements

Force measurements for four different velocities are plotted and compared in figure 4. For all but the lowest velocity at $U=0.05 \text{ m/s}$ the force measurements for the lower filling levels are substantially

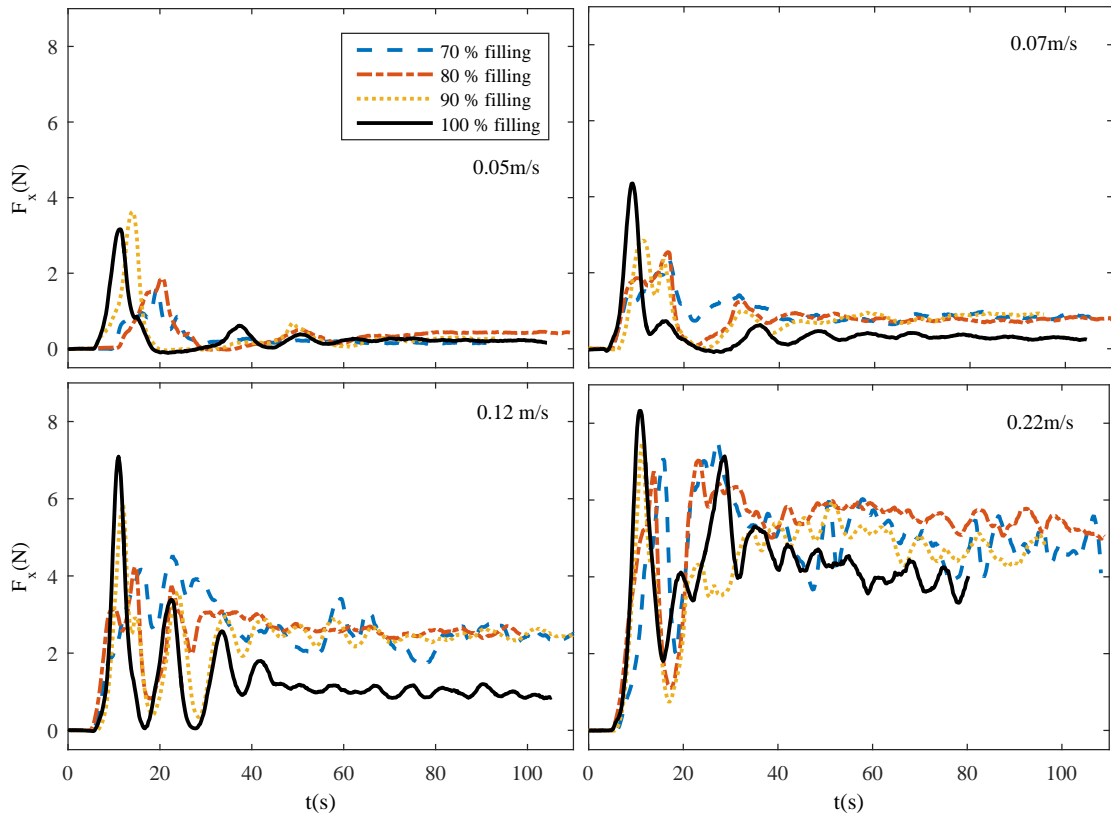


Figure 4: Comparison plot of force measurements for four different current, $U=0.05$ m/s, 0.07 m/s, 0.12 m/s and 0.22 m/s, for all the four filling levels, from the May 2013 experiments.

higher than the 100 % filling level. All the drag force measurements indicate that the drag force is dependent on the filling level.

Some oscillations are observed in the force measurement time series. They are small for the three smallest presented velocities. However, for the 0.22 m/s velocity the oscillations are large, especially for the 70 % filling level.

3.2. Bag deformations

A hemispherical cup was seen forming at the front when the bag was exposed to current, for $U \geq 0.07$ m/s, as illustrated in figure 5 right part. The deformation is shown for the 80% filling level in figure 5 left part, and the hemispherical cup is indicated with the black dotted line. This deformation increase as the filling level decreases and the current velocity increases, see figure 7. In figure 7, images from the two cameras are shown for the same velocities as the force measurements. The images are taken within the middling time interval around $t=60$ s. The image material shows that the bag deforms for all filling levels. The deformations appear to be dependent on both filling level and velocity. For filling levels below 100 % a large deformation of the front can be observed for all $U \geq 0.07$ m/s. This deformation is consistent with the local deformation pattern described by Rudi and Solaas (1993) shown in figure 1(b) left part, and what have been found for other geometrical shapes in Strand et al. (2013) and Lader et al. (2015). For the 100 % filling level we observe small deformations, but these deformations do not appear to effect the drag forces.

For $U \leq 0.05$ m/s ($Re \leq 4 \cdot 10^4$), the bag did not appear to reach a fully deformed shape, but

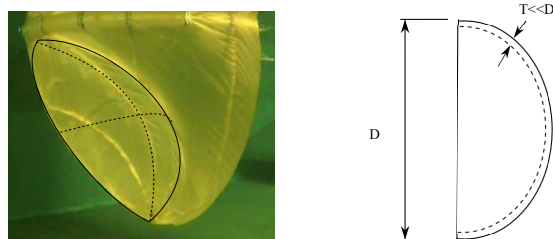


Figure 5: Left: Deformation pattern of the CFC at $U = 0.12$ m/s at filling level 80%. Primary deformation indicated with lines. Right: Illustration of thin hemispherical cup. Illustration adapted from Blevins (1984)

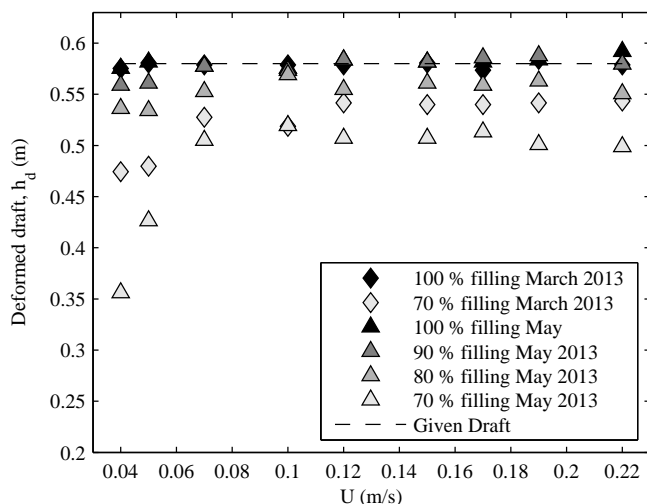


Figure 6: Measured deformed draft for bag exposed to current at different filling levels.

stayed closer to the initial zero velocity shape. This was also an effect which was found for the same velocity range in Strand et al. (2013) for a cylindrically shaped bag.

The back wall relative to the current were observed deforming only for the very highest velocities. This can be seen on the images of all the filling level at the 0.22 m/s current velocity in figure 7, where the back wall of the bag deforms out of the borders of the reference. Deformation of the back wall is in accordance with the global current deformations described by Rudi and Solaas (1993), and contrary to Strand et al. (2013) which studied a circular bag. The reason why these deformations were not found in Strand et al. (2013) can be that lower current velocities were considered.

Measurements of the draft of the deformed bag indicate a decrease in draft for lower filling levels. This can also be seen when the contour of the zero current 100 % filling level is compared to the deformed shape of the bag in figure 7. The deformed draft in the images was estimated using equation 1, and plotted in figure 6. The plot indicates a general significant decrease in draft, and subsequently a decrease in exposed area for decreasing filling levels. The magnitude of the draft appears close to constant within each filling level, for $U \geq 0.07$ m/s. The decrease in draft for decreasing filling levels were also found for a cylindrical bag in Strand et al. (2013).

For the May 2013 experiments the videos show an oscillatory behaviour with fluttering in the front facing the current. The drag measurements from these velocities also showed the same tendencies by exhibiting a larger standard deviation and more peaks in the force measurement, within the middling time, see figure 8. If the force measurement plot is compared to the images taken at the marked time instances, only small variations in shape can be observed. No general clear direct connection between

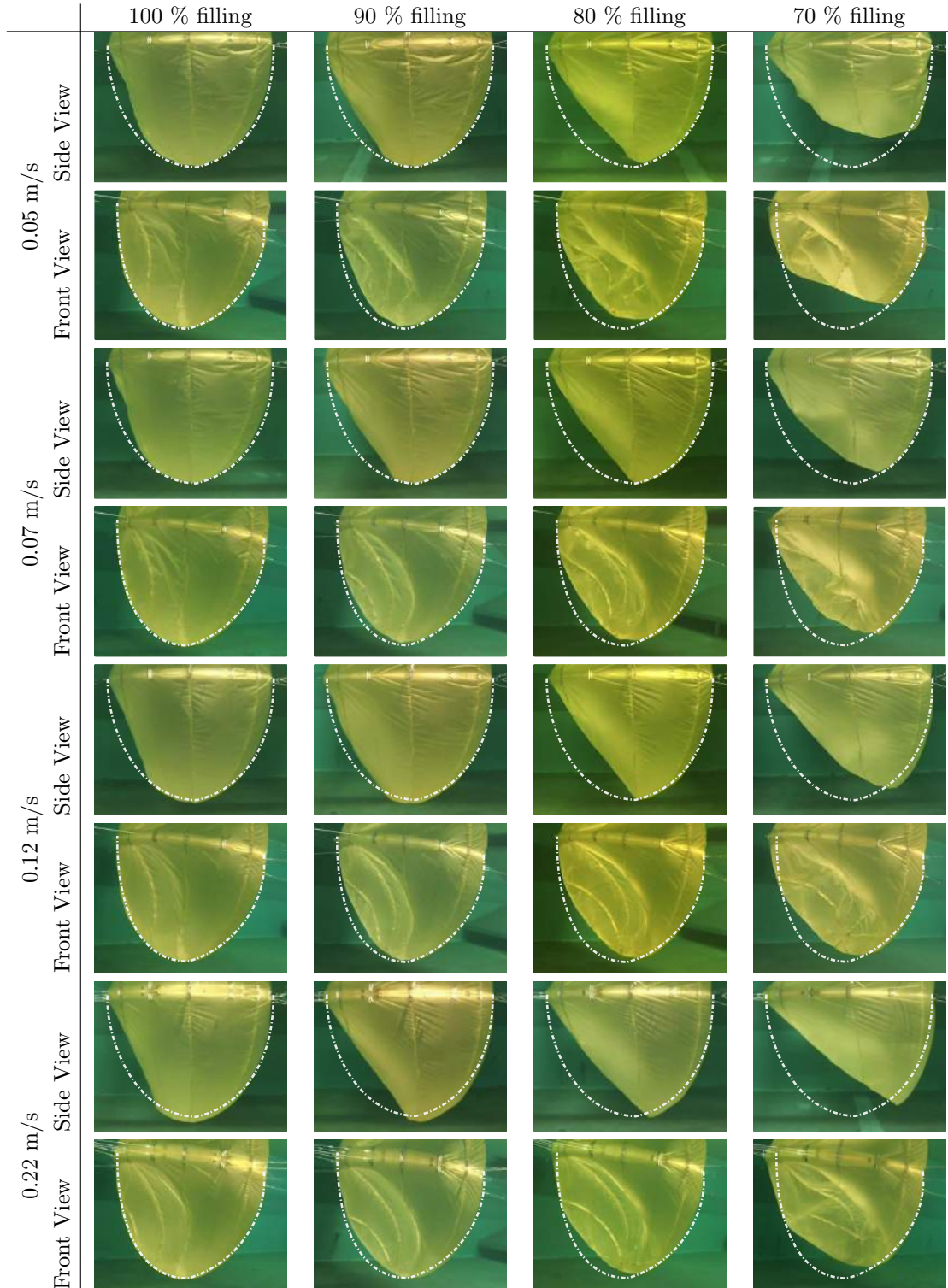


Figure 7: Image material, camera 1 (Side View) and 2 (Front View), taken during the May 2013 experiments. Deformation patterns for 100 %, 90 %, 80 and % 70 % filling levels, for selected current velocities from 0.05 m/s to 0.22 m/s. 100 % filling level 0 m/s used as reference, see white dotted line.

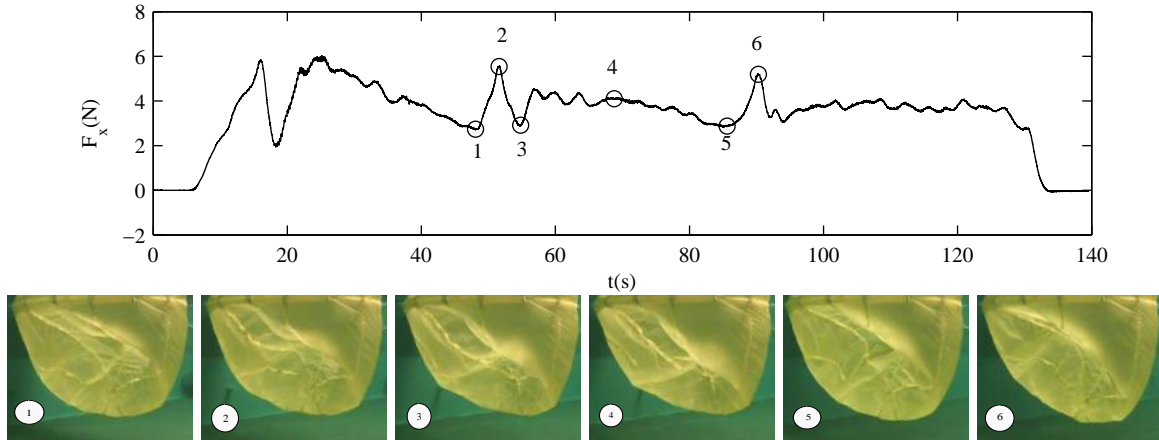


Figure 8: Topp: Force measurement time series for 70 % filling level at $U=0.15$ m/s. Bottom: Images from camera 2 (Front view) taken at the time instances 1-6, marked in the time series. Only small changes in the geometry can be observed. From the May 2013 experiments.

the images and the time series can be seen, as it appear to be only small differences in the shape for image 1-3. Although, within this time period a force variation of 3 N can be observed for the force measurements. Image 2 and 6, which are the images taken at the force peaks could appear to have a slightly larger deformed draft and a deformation with fewer wrinkles in the center, but the differences compared to remaining images are as earlier mentioned small. The presented measurement was taken at 0.15 m/s, at higher velocities both the time series and the videos of the bag appeared more chaotic. This can be seen in the times series at 0.22 m/s in figure 4.

The increase in drag force on the bag appear to happen simultaneously as the large deformations for lower filling levels appear. The density of the water is kept constant and the velocity is known. Both the drag coefficient and the projected area in eq. 2 are dependent on the deformed shape of the bag. The projected frontal area of the bag is decreasing for decreasing filling levels. It is therefore plausible that the increase in drag is caused by the change in shape, effecting the drag coefficient.

3.3. Drag Forces

Reduced data for all the filling levels at all the velocities are plotted in figure 9. Error bars are included to indicate the variation in the force measurement within the middling time interval. The error bars on the measurement points are calculated based on the standard deviation of the measurement time series within the middling time.

The solid lines in figure 9 are the empirical drag given by eq. 2 with constant area A and the drag coefficient C_D . The drag coefficient used here is the empirical mean drag for a sphere which is $C_D = 0.47$ at $Re = 10^5$ (Hoerner, 1958). An half ellipsoid and a sphere are different, and the free surface is known to have an effect on the drag coefficient. However, since no other comparison drag coefficient were found more appropriate, a sphere will be used. The dashed line interval is the drag coefficient range for a hemispherical cup at $C_D = [1 - 1.42]$ given by Hoerner (1958). This interval is based on decreasing the depth over diameter ratio of a hemispherical cup from a deep hemispherical cup where $C_D = 1.42$, until the drag coefficient of a flat plate/disk where $C_D = 1$.

An increase in drag is observed for decreasing filling levels for all velocities, see figure 9. When the drag force measurements are compared with eq. 2, the drag force seem to be proportional to U^2 , independent on the filling level. The solid line, based on the sphere drag coefficient captures the trend for the drag at the 100 % filling level. When the filling level decreases, the trend changes, such that the measurement points appear to be within the hemispherical cup interval given by Hoerner (1958). This results are comparable related to other geometries presented in Strand et al. (2013) and Lader et al.

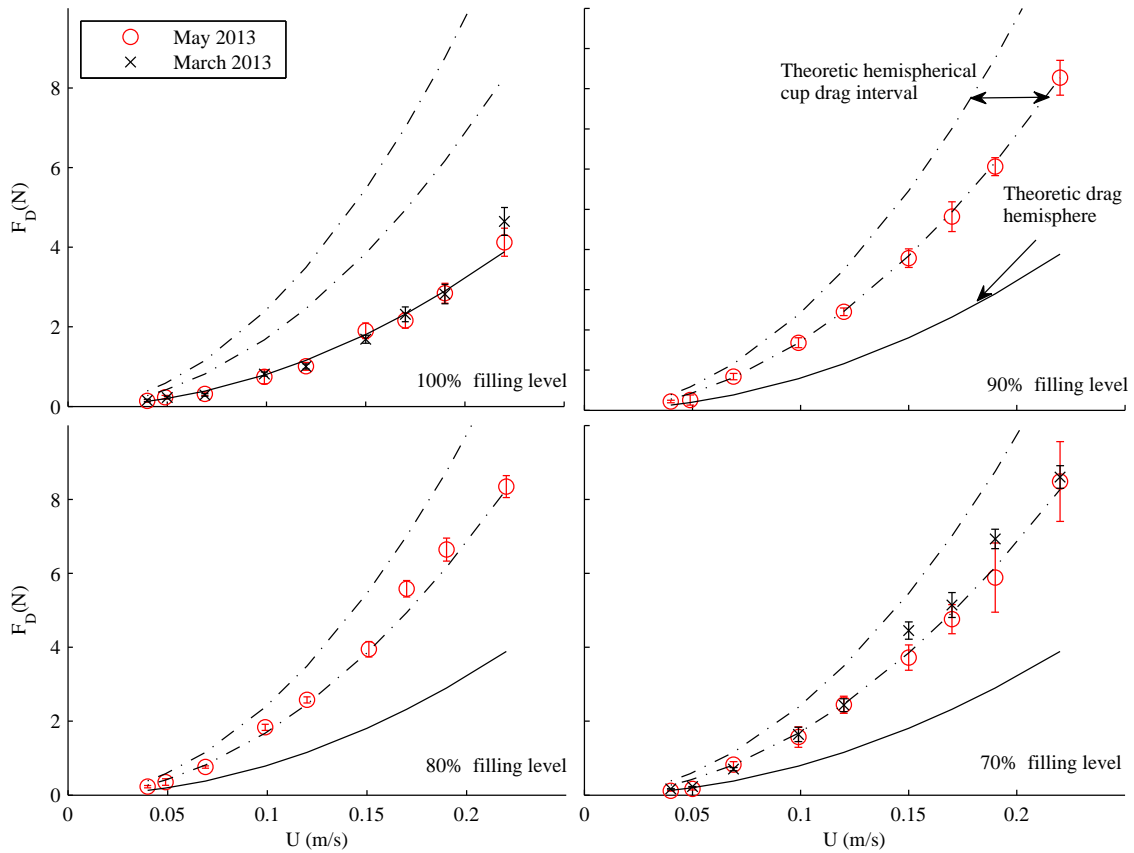


Figure 9: Plot of drag forces found from all the experiments, for 100%, 90%, 80 % and 70 % filling level. Solid line gives theoretic drag for a sphere, and dotted line interval gives the theoretic hemispherical cup drag interval, given by (Hoerner, 1958).

(2015). For the lower filling levels the bag displayed large deformations of the shape, simultaneously as the drag forces on the bag increased, though to a smaller level than earlier published.

The error bars in figure 9 reflect the standard deviation of the measurements within the middling interval. The May 2013, 70% filling level deviates from the general trend, with a larger standard deviation.

3.4. Drag coefficient

The undeformed projected area $A = \pi hD/4$ was used in the calculation of the drag coefficient C_D . C_D was plotted against the Reynolds number in figure 10 for all the filling levels.

The drag coefficient reflects the observed deformation patterns, supporting the theory of a significant increase in drag coefficient for decreasing filling levels. Figure 10 indicates a drag coefficient close to the empirical drag coefficient of a sphere of 0.47 for the 100% filling level (Hoerner, 1958). The drag coefficient C_D increases up to the interval for the hemispherical cup given by Hoerner (1958) for the filling levels under 100%.

For $Re \leq 4 \cdot 10^4$, at filling levels below 100 % the drag coefficients are lower than the drag coefficients at higher Reynolds numbers. Hence, that the bag does not deform will have an effect on the drag coefficients, which can also be observed in figure 10. The drag coefficient at the 70 % filling level is considerably smaller than the rest of the Reynolds numbers for the lowest filling levels at the lowest Reynolds numbers, $Re < 5 \cdot 10^4$. Since the large cup deformation have not appeared, and the draft is small, it is plausible that the drag coefficient is smaller.

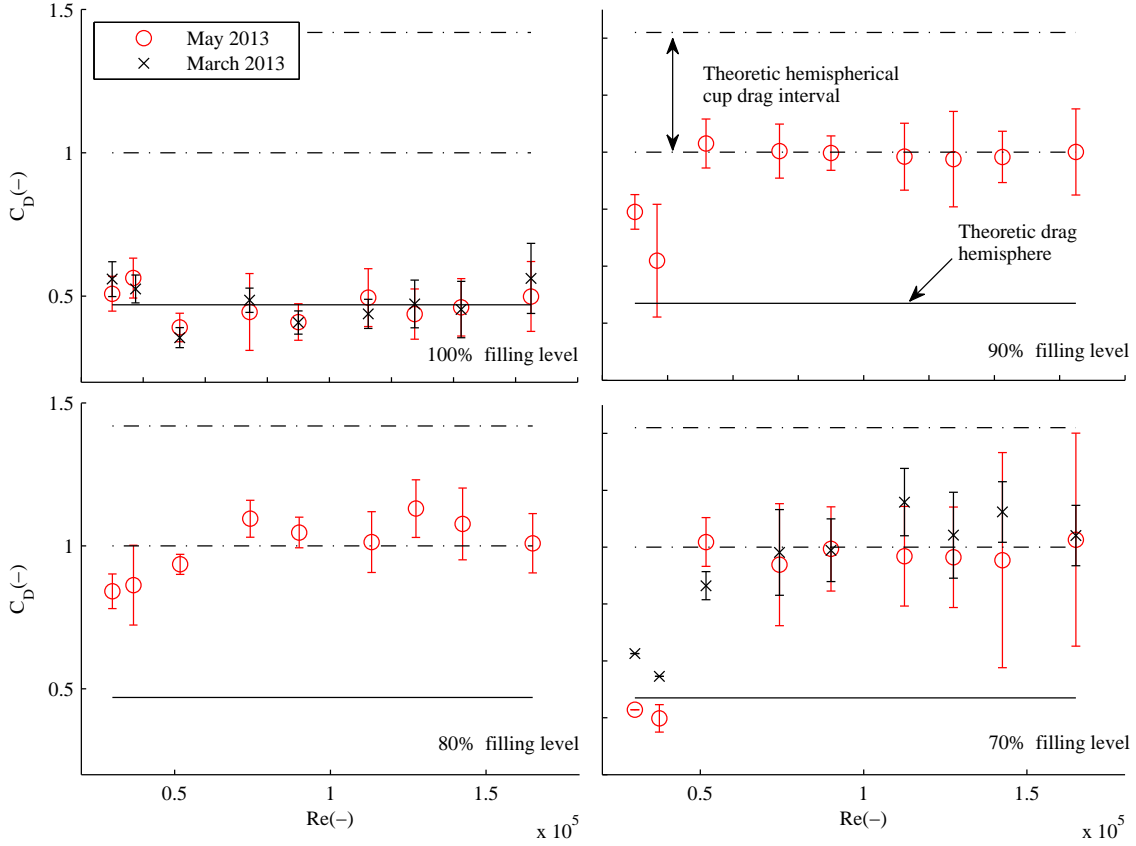


Figure 10: Plot of drag coefficients C_D for all the experiments, for 100%, 90%, 80 % and 70 % filling level. The solid line gives theoretic drag coefficient for a sphere, and dotted line interval gives the drag coefficient interval for a thin hemispherical cup, given by (Hoerner, 1958).

For the 70- 90% filling level for $Re > 4 \cdot 10^4$, the drag coefficient increases to the drag coefficient interval for the hemispherical cup, see figure 10 and table 2. This is consistent with the deformation patterns observed in section 3.2, for velocities over $Re \geq 4 \cdot 10^4$, which is when the characteristic hemispherical cup have appeared. The trend of the measurement points appears to approach a constant value. C_D appears close to constant also for the 70% filling level, for $Re > 11 \cdot 10^4$, despite the observed oscillations in shape and forces. This indicates that these oscillations do not have a significant effect on the mean force. However, the standard deviation indicated by the error bars have grown substantially larger, see figure 9.

The presented experimental results also indicate a quick transition in drag coefficient between 90 and 100 % filling level. This is a much more rapid change than what was found in Lader et al. (2015) and Strand et al. (2014), where the change in drag coefficient appeared to happen more gradually related to the filling level. Only one run for each filling level were reported for these experiments for each geometry. However, since only one run was reported for the presented experiments for the 80 and 90 % filling level, no firm conclusions of the transition filling level can be made.

Mean drag coefficients ($\overline{C_D}$) were calculated for each individual filling level λ for each experimental series, and are given in table 2. Three different mean drag coefficients have been calculated, one general mean using all the data points and two mean drag coefficients divided by Reynolds number, one for $Re \leq 4 \cdot 10^4$ ($\overline{C_{D\leq}}$) and one for $Re > 4 \cdot 10^4$ ($\overline{C_{D>}}$). This division is based on the observed deformation patterns and also the trend of the drag coefficients in figure 10.

The mean drag coefficient ($\overline{C_D}$) for all the filling levels below 100 % are either within or close to the

Table 2: Mean drag coefficients for the experiments conducted in March and May 2013. $\overline{C_D}$ is the mean drag coefficient for all the data points within a filling level. $\overline{C_{D\leq}}$ is the mean drag coefficient for $Re \leq 4 \cdot 10^4$ and $\overline{C_{D>}}$ is the drag coefficient for $Re > 4 \cdot 10^4$.

| | $\overline{C_{D\leq}}$ | 70 % $\overline{C_{D>}}$ | $\overline{C_D}$ | $\overline{C_{D\leq}}$ | 80 % $\overline{C_{D>}}$ | $\overline{C_D}$ | $\overline{C_{D\leq}}$ | 90 % $\overline{C_{D>}}$ | $\overline{C_D}$ | $\overline{C_{D\leq}}$ | 100 % $\overline{C_{D>}}$ | $\overline{C_D}$ |
|-------|------------------------|-----------------------------|------------------|------------------------|-----------------------------|------------------|------------------------|-----------------------------|------------------|------------------------|------------------------------|------------------|
| March | 0.59 | 1.03 | 0.93 | - | - | - | - | - | - | 0.54 | 0.45 | 0.47 |
| May | 0.41 | 0.98 | 0.85 | 0.85 | 1.04 | 1.00 | 0.70 | 1.00 | 0.93 | 0.54 | 0.45 | 0.47 |

hemispherical cup interval. All the means are affected by the first two measurement points, reducing the value. If we consider the mean drag for $Re > 4 \cdot 10^4$, the mean drag is increased relative to the total mean ($\overline{C_D}$). The mean drag coefficient for the 100 % filling level for the March and May 2013 experiments are equal. For the 70 % filling level, $\overline{C_D}$ is lower for the May 2013 experiments than for the March 2013 experiments. From section 3.2 we observed that the draft were smaller for the May 2013 experiments, which would influence the drag, and thereby the drag coefficient. It should be taken into consideration that figure 6 shows that the deformed draft is less than the undeformed draft. This would have an effect on the actual drag coefficient, resulting in a further increase of the drag coefficients for the lower filling levels.

4. Discussions

The repeatability of the results are viewed as acceptable. The difference in mean drag force between the March and May 2013 experiments for the 100% filling level is within 1% and within 6% for the 70% filling level.

The CFFC is a complex system, and for the presented experiments we have limited to no information of the fluid flow inside and around the CFFC during the experiments. We have observed a complex interaction between the membrane, the fluid masses within the CFFC and the outside fluid flow. To have better control of all variable it would have been useful to also have information about the tension in the fabric and the fluid flow around and inside the CFFC.

4.1. Experimental results

It can then be questioned if the bag deformations have not had time to develop, due to slow dynamics for $U=0.04$ m/s and $U=0.05$ m/s. However, when the force measurement were examined directly with the emphasise of slow changes, no changes were found within the middling time interval. Both the 0.04 m/s and the 0.05 m/s velocity have low variance in the force measurements after the transient period. The 0.07 m/s velocity exhibits a quick change in geometry during the transient phase, before stabilising at a higher drag force level with the deformation pattern seen in the higher velocities.

It appears to be a significant difference between the 70 % filling level drafts of the May and March 2013 experiments. Both the first two velocities, but also the mean is lower for the May 2013 experiments. These results can indicate that filling level is smaller than intended. The differences in shape and deformed drafts (see figure 6) between the March and May 2013 for the lowest velocities in the range $U \leq 0.05$ m/s ($Re \leq 4 \cdot 10^4$), can be explained by different initial shape. Strand et al. (2014) reported large variations in shape and connected draft for the 70% filling level at zero current, still water, and for these velocities the shape does not appear to change much from the static shape, as also seen in Strand et al. (2013).

For velocities above 0.12 m/s for the 70 % filling level, in the May 2013 experiments, the deformation in front became unsteady. This does not happen for the March 2013 experiments. If the lower draft for the May 2013 experiments indicates a lower than intended filling level, the oscillations can indicate that a new phenomenon appears when the filling level reaches some level below 70 %. What can be

the reason for that the front of the CFFC becomes unsteady? And how can these small oscillations be the cause of the large variations in drag seen in figure 8? One possible explanation can be found if we look at parachutes. The shape of parachutes are known to oscillate under some unfavourable conditions (Hoerner, 1958). The oscillation of the shape/diameter is called "breathing", and is caused by the interaction between the near-wake fluid forces and the fabric (Johari and Desabrais, 2005). This behaviour leads to a fluctuation in the drag force, and is associated with a clear vortex shedding frequency in the response. The fluctuations in the drag have been reported to be up to 27 % of the mean, see Johari and Desabrais (2005). The standard deviations compared to the mean drag force for the presented results were 10-16% above the mean. For parachutes most of this drag fluctuations are associated with added mass fluctuations. The time series of the performed experiments were too short to capture any dominant vortex shedding frequency, in order to prove that this could be the case for the CFFC. To further study this phenomenon more information about the flow inside and around the CFFC, and a longer towing tank than the MC-Lab is needed.

The increase in drag coefficient for the presented experiments are lower than the increase found for decreasing filling levels for other geometries in Strand et al. (2013) and Lader et al. (2015). However, in Strand et al. (2013) and Lader et al. (2015) shorter time series were used, and the experiments were run in series with three velocities in each run, 120 s in total. In the experiments presented here the time series are between 90 and 120 s long. Sarpkaya (2010) studied the effect of travelled distance on a circular cylinder in an impulsively started flow. He defined non-dimensional travelled distance as L/r , where $L = Ut$ and r is the radius of the cylinder. He found that the drag coefficient in the initial stages ($Ut/r \leq 4$) of an impulsively started flow can exceed its steady value by as much as 30%. Sarpkaya (2010) defined a transient interval between $L/r \approx [0, 17]$ for Reynolds numbers from $10^4 - 10^5$. The same phenomenon have been found for spheres, with the same tendency to overshoot the stationary drag coefficient in the transient phase, but with a longer transient phase (Roos and Willmarth, 1971). For the March and May 2013 experiments we get $L/r \in [9, 64]$, where all the velocities except $U=0.04$ m/s and $U=0.05$ m/s are outside the transient range. The results reported by Strand et al. (2013) and Lader et al. (2015) are in the range $L/r \in [4, 19]$. This could indicate that the larger drag coefficients found in Lader et al. (2015) and Strand et al. (2013) are due to effects of transients on the drag coefficients.

4.2. Error Sources

Blockage effects have been shown to have an effect on the drag coefficient for large blocking ratios, see e.g Maskell (1965). The blockage ratio is calculated as the projected area of the bag (0.34 m^2) divided by the tunnel cross-section area in the towing direction ($9.03-9.68 \text{ m}^2$). The largest blockage ratio was 3.8% for the presented experiments. West and Apelt (1982) have carried out a study of the effect of blockage on the drag coefficient for a circular cylinder in the Reynolds number range $[10^4 - 10^6]$. They concluded that for blockage ratios less than 6% the effect on the drag coefficient was small.

The results presented in this paper showed that the drag force is highly dependent on the filling level of the bag. The bag was to some extent permeable. For parachutes, drag have been shown to be dependent on the permeability of the fabric (Hoerner, 1958). The permeability of the nylon used in the experiments were not measured, but since parachute nylon were used it will be assumed that the permeability is not far from 1-2% (Johari and Desabrais, 2005). Permeability at this level can lead to a small reduction in the drag compared to non permeable structures. The filling level of the bag was measured after each experiment. However, the flow meter have an error of 3 % and the measured filling level were in addition for the May 2013, 70 % filling level, 4 % lower than the intended filling level. If this error have accumulated in the same direction, the filling level could have been 7% less than intended, something which would influence the results.

4.3. Application to full scale

Typical full scale current velocities at aquaculture sites in Norway are in the range $U_c = 0.1-1.0$ m/s. Ideally for this results to be applicable to full scale dimensions, we should have equality in Reynolds

numbers. However, due to known physical and economical limitations of the towing tank, this is not feasible (Hoerner, 1958). To transfer the results to full scale, Froude scaling was used. The Froude number is given as $Fn = V/\sqrt{gl}$ and is normally used in relation with free surface flows. When geometric scale $\tau = D_M/D_F$, where D_M is the model scale diameter and D_F is the full scale diameter, we have experimental data covering the scaling range from $\tau = 1:17$ to $1:50$. These scales corresponds to full scale diameters used by the aquaculture industry in Norway today from 13-38 m.

Model current velocities will not give equality in Reynolds number between model and full scale. The Reynolds number interval for full scale current velocities gives $Re = [10^6 - 10^7]$, while the Reynolds numbers in model scale are in the interval $Re = [10^4 - 10^5]$. The drag coefficient is known to be dependent on both the transition to turbulent flow, which again are dependent on the Reynolds Number, the geometry and the material of the structure (Blevins, 1984). For the lower filling levels the bag was observed to deform, introducing changes in the bag geometry. Blevins (1984) stated that when sharp corners are introduced, the drag coefficient was independent of Re for $Re > 10^4$. This makes the drag coefficient scalable for these conditions, since the drag coefficient is pressure drag dominated and mainly dependent on the placement of the separation point for clearly defined separation points. However, this requires that the large front deformation have appeared. From the results we have seen that for $Re \leq 4 \cdot 10^4$ the characteristic deformation in front do not appear. When the hemispherical cup appears in full scale in terms of Reynolds number cannot be decided. However, the most critical condition in terms of drag loads, must be when the large front deformation appears. The largest drag force should be ruling for the dimensioning of mooring of the CFFC, this would then be when the large hemispherical cup have appeared.

In general it is required for an elastic model that elastic similarity for the material is satisfied (Løland and Aarsnes, 1994). Requiring that $E_M t_M = E_F t_F / \tau^2$, where subscript M denotes model, and subscript F denotes full scale. The CFFC is made of a fabric with a low E-modulus (low in-plane stiffness). It have not been possible to find a usable material i model scale that satisfies the elastic similarity condition. With $E_M \approx E_F$, $t_M = 0.05$ mm and $t_F \approx 1$ mm, the bag fabric is 100-1000 times to stiff in model scale. No literature was found regarding the scaling-effects of the stiffness of the fabric on drag for CFFCs. The effect of scaling of in plane stiffness on parachutes in water have however, been investigated. It has been found that the overall geometry of a parachute is not much affected by the stiffness of the fabric (Johari and Desabrais, 2005). The drag force on the bag is highly dependent on the global shape of the bag. Since the shape is not affected by the fabric stiffness, this will most probably not have an influence on the application of the results to full scale.

5. Conclusions

To utilize Closed Flexible Fish Cage technology at an industrial level more knowledge is needed about the effect of sea loads. Drag forces on a CFFC for different filling levels and current velocities have been experimentally studied. A significant increase in drag was experienced as the filling level decreased. This drag increase was found to be due to a large deformation of the front wall facing the current, leading to a significant increase in the drag coefficient. The largest drag force should be ruling for the dimensioning of mooring of the CFFC. This would then be when the large hemispherical cup have appeared. To better predict the forces and deformations on the bag, numerical models taking into account the dependency between force and deformation should be developed.

6. Acknowledgements

This work have been financed by the Research Council of Norway through the project "External Sea Loads and Internal Hydraulics of Closed Flexible Cages" (grant no. 216127). The work has been carried out at the Centre for Autonomous Marine Operations and Systems (AMOS), supported by the Research Council of Norway through the Centres of Excellence funding scheme, project number 223254 - AMOS. The Norwegian Research Council is acknowledged as the main sponsor of AMOS. The authors thank professor O.M. Faltinsen for his guidance and contribution.

References

- R.D. Blevins. *Applied fluid dynamics handbook*. Van Nostrand, New York, 1984.
- W.R Hawthorne. The early development of the dracone flexible barge. In *Proceedings of the Institution of Mechanical Engineers 1847-1982*, 1961.
- S. Hoerner. *Fluid-Dynamic Drag*. Midland Park, NJ, 1958.
- H. Johari and K.J. Desabrais. Vortex shedding in the near wake of a parachute canopy. *Journal of Fluid Mechanics*, 536:185 – 207, 2005.
- Trygve Kristiansen and Odd M. Faltinsen. Experimental and numerical study of an aquaculture net cage with floater in waves and current. *Journal of Fluids and Structures*, 54:1–26, 2015.
- Pål Lader, David W. Fredriksson, Zsolt Volent, Jud DeCew, Trond Rosten, and Ida M. Strand. Drag Forces on, and Deformation of, Closed Flexible Bags. *Journal of Offshore Mechanics and Arctic Engineering*, 137(August):041202, 2015.
- G. Løland and J.V. Aarsnes. Fabric as construction material for marine applications. In *Hydroelasticity in marine technology*, 1994.
- E. C. Maskell. A theory of the blockage effects on bluff bodies and stalled wings in a closed wind tunnel. Technical report, AERONAUTICAL RESEARCH COUNCIL LONDON (UNITED KINGDOM), 1965.
- E. P. Michael, G. Chadwick, J. Parsons, and Boumy Sayavong. Evaluation of closed - containment aquaculture. In *Evaluation of closed - containment technologies for saltwater salmon aquaculture*. Ottawa : NRC Research Press, 2010.
- F. W. Roos and W. W. Willmarth. Some experimental results on sphere and disk drag. *AIAA Journal*, Vol.9(2):285–291, 1971.
- T Rosten, B. F. Terjesen, Y. Ulgenes, K. Henriksen, E. Biering, and U. Winther. More knowledge is needed about aquaculture in closed fish farms at sea (in norwegian). *Vann*, (1):5–13, 2013.
- H. Rudi and F Solaas. Floating fish farms with bag pens. In *International Conference on Fish Farming Technology*, 1993.
- T. Sarpkaya. *Wave Forces on Offshore Structures*. Cambridge University Press, 2010.
- I.M. Strand, A.J. Sørensen, P. Lader, and Z Volent. Modelling of drag forces on a closed flexible fish cage. In *9th IFAC Conference on Control Applications in Marine Systems. Osaka, Japan*, 2013.
- I.M. Strand, A.J. Sørensen, and Z. Volent. Closed flexible fish cages: Modelling and control of deformations. In *Proceedings of 33rd International Conference on Ocean, Offshore and Arctic Engineering. June 8-13, 2014, San Francisco, USA*, 2014.
- G.S. West and C.J. Apelt. Effects of tunnel blockage and aspect ratio on the mean flow past a circular cylinder with reynolds numbers between 10^4 and 10^5 . *Journal of Fluid Mechanics*, 114:361 – 377, 1982.
- R. Zhao. A complete linear theory for a two-dimensional floating and liquid-filled membrane structure in waves. *Journal of Fluids and Structures*, 9(8):937–956, 1995.